Oxidized low-density lipoprotein receptor 1: a novel potential therapeutic target for intracerebral hemorrhage

https://doi.org/10.4103/1673-5374.332157

Date of submission: May 7, 2021

Date of decision: September 9, 2021

Date of acceptance: November 3, 2021

Date of web publication: January 7, 2022

Hui-Yuan Zhang, Xi Lu, Yue-Han Hao, Ling Tang, Zhi-Yi He*

From the Contents

Introduction	1795
Materials and Methods	1796
Results	1797
Discussion	1799

Graphical Abstract *Oxidized low-density lipoprotein receptor 1 silence ameliorates the secondary brain injury in intracerebral hemorrhage through blocking ferroptosis by inhibiting the p38 signaling pathway*

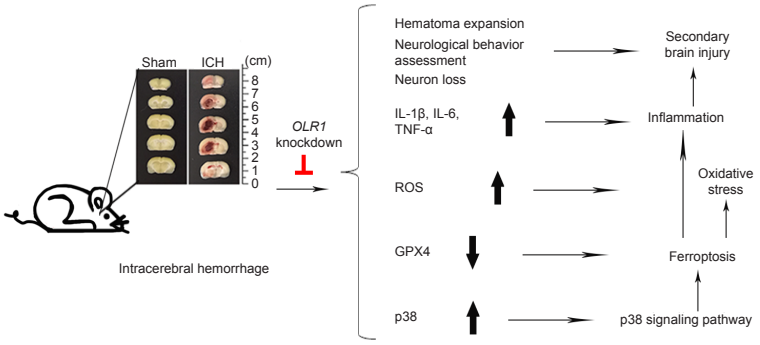

Abstract

Oxidized low-density lipoprotein receptor 1 (OLR1) is upregulated in neurons and participates in hypertension-induced neuronal apoptosis. *OLR1* deletion exerts protective effects on cerebral damage induced by hypertensive-induced stroke. Therefore, OLR1 is likely involved in the progress of intracerebral hemorrhage. In this study, we examined the potential role of OLR1 in intracerebral hemorrhage using a rat model. *OLR1* small interfering RNA (10 μL; 50 pmol/μL) was injected into the right basal ganglia to knock down *OLR1*. Twenty-four hours later, 0.5 U collagenase type VII was injected to induce intracerebral hemorrhage. We found that knockdown of *OLR1* attenuated neurological behavior impairment in rats with intracerebral hemorrhage and reduced hematoma, neuron loss, inflammatory reaction, and oxidative stress in rat brain tissue. We also found that silencing of *OLR1* suppressed ferroptosis induced by intracerebral hemorrhage and the p38 signaling pathway. Therefore, silencing *OLR1* exhibits protective effects against secondary injury of intracerebral hemorrhage. These findings suggest that OLR1 may be a novel potential therapeutic target for intracerebral hemorrhage.

Key Words: ferroptosis; inflammation; intracerebral hemorrhage; neurological behavior; neuroprotection; novel therapeutic target; oxidative stress; oxidized low-density lipoprotein receptor 1; p38 signaling pathway; secondary brain injury

Introduction

Intracerebral hemorrhage (ICH) is a devastating nervous system disease with high mortality and disability rates and constitutes approximately 15% of stroke cases worldwide (Rocha et al., 2020). Approximately 75% of survivors with persistent ICH show various degrees of neurological function deficit, including sensory, reflex, motor, and language deficits (Ren et al., 2020a). Cerebral damage induced by ICH is not only from hematoma expansion and hematoma mass effects (the main reasons of primary damage), but also from secondary brain injury (Chen et al., 2015; Wang et al., 2018; Deng et al., 2020). Secondary damage is caused by intraparenchymal blood, resulting in activation of excitotoxic, cytotoxic, inflammatory, and oxidative pathways, and hemoglobin lysate (including iron) released from hematoma (Zhou et al., 2014; Wan et al., 2019). An effective treatment for ICH is lacking because of the complex pathophysiology of ICH (Sembill et al., 2018). Thus, better understanding of the underlying mechanisms is critical to identify novel therapeutic targets for ICH.

Iron released from hematomas can cause an oxidative threat to surrounding tissues, resulting in an iron-dependent non-apoptotic cell death known as ferroptosis (Zhang et al., 2018; Djulbegovic and Uversky, 2019; Stockwell et al., 2020). Ferroptosis is characterized by extremely high lipid peroxidation levels and contributes to secondary brain injury after ICH (Djulbegovic and Uversky, 2019; Bao et al., 2020; Zhang et al., 2020b; Fan et al., 2021). In the ferroptosis process, the repression of glutathione peroxidase 4 (GPX4) enhances lipid peroxide production, leading to increased reactive oxygen species (ROS), which causes oxidative lipid damage and ferroptosis of neuronal cells (Guo et al., 2017; Bai et al., 2019). Glutathione (GSH) acts as the reducing substrate for GPX4 activity and is indispensable for inhibiting ferroptosis (Feng and Stockwell, 2018). A previous study showed that the amelioration of ferroptosis in the acute phase

Department of Neurology, The First Hospital of China Medical University, Shenyang, Liaoning Province, China
*Correspondence to: Zhi-Yi He, PhD, hezhiyi0301@sina.com.
https://orcid.org/0000-0002-0995-0294 (Zhi-Yi He)

Funding: *This study was supported by the National Natural Science Foundation of China, No. 81971125 (to ZYH).*
How to cite this article: *Zhang HY, Lu X, Hao YH, Tang L, He ZY (2022) Oxidized low-density lipoprotein receptor 1: a novel potential therapeutic target for intracerebral hemorrhage. Neural Regen Res 17(8):1795-1801.*

of ICH exerts long-term cerebral protective effects by decreasing malondialdehyde (MDA) and cyclooxygenase-2 (COX-2) levels (Chen et al., 2019). Therefore, identifying treatments targeting ferroptosis might be an excellent strategy against the progression of ICH.

Oxidized low-density lipoprotein receptor 1 (OLR1), also known as lectin-like oxidized low-density lipoprotein receptor-1 (LOX-1), is a membrane protein receptor of the C-type lectin family (Akhmedov et al., 2021; Barreto et al., 2021). OLR1 is mainly expressed in organs with abundant blood vessels, such as placenta, lung, and brain, and plays an essential role in vascular dysfunction (Shaw et al., 2014). OLR1 is upregulated in neurons and involved in hypertension-induced neuronal apoptosis (Li et al., 2012). OLR1 deletion exerts protective effects on cerebral damage induced by hypertensive-induced stroke (Liang et al., 2020). Bioinformatics analysis predicted that ORL1 is highly expressed in hematoma tissues after ICH and ORL1 is a biomarker of acute ICH (Inoue et al., 2019; Liu et al., 2019). We thus speculated that OLR1 might play a role in post-ICH brain injury.

In this study, we investigated the function of OLR1 in cerebral damage in ICH. We established an ICH mouse model using collagenase type VII to explore the role of OLR1 in brain injury and examined the underlying mechanism of the cerebral protection caused by downregulated OLR1.

Materials and Methods

Animals

All animal experimental protocols were approved by the Institutional Animal Care and Use Committee of China Medical University (approval No. KT2018042; approval date: March 1, 2018) and were performed in compliance with The Guideline for the Care and Use of Laboratory Animals. All experiments were designed and reported according to the Animal Research: Reporting of *In Vivo* Experiments (ARRIVE) guidelines (Percie du Sert et al., 2020). Adult male Sprague-Dawley rats (280–320 g; 8 weeks old) were purchased from Liaoning Changsheng Biotechnology (Benxi, China; lisense No. SCXK (Liao) 2020-0001). Only male rats were obtained to avoid any unknown effects because of sex (such as the influence of estrogen). Animals were maintained under controlled temperature (22 ± 1°C) and humidity (45–55%) conditions and a 12-hour light/dark cycle. Rats were randomly divided into four groups (sham, ICH, ICH + scramble siRNA, and ICH + OLR1 siRNA groups; 30 rats per group). In each group, six rats each were used for brain water content detection, histological analysis, molecular experiments, ROS detection, and detection of inflammatory factors and oxidative stress-related factors in the subsequent experiments.

Intracerebral hemorrhage model and oxidized low-density lipoprotein receptor 1 knockdown

The ICH model was induced with collagenase type VII (MilliporeSigma, Billerica, MA, USA) as described previously (Zhang et al., 2020a). Briefly, rats were anaesthetized by an intraperitoneal injection with sodium pentobarbital (Xiya Reagent, Shandong, China) at a dose of 50 mg/kg, then supinely fixed in a stereotaxic fame (Shanghai Alcott Biotech, Shanghai, China). A burr hole (1 mm) was made in the skull (0.2 mm in front of the bregma, 3 mm right lateral to midline, and at a 6-mm depth below the skull) with a dental drill. Next, 0.5 U collagenase type VII was infused into the right basal ganglia (Paxinos and Watson, 1986) at a rate of 0.4 μL/min (Xi et al., 2018; Ouyang et al., 2019). The needle was held in place for 10 minutes after infusion to prevent blood leakage. The hole was then sealed with bone wax and the wound was sutured. Rats in the sham group were infused with an equal volume (2 μL) of saline instead of collagenase type VII through the burr hole.

For the knockdown of OLR1, rats were supinely fixed in a stereotaxic fame after anaesthetization. A burr hole (1 mm) was made in the skull (1 mm behind the bregma and 1.5 mm right lateral to midline) with a dental drill. OLR1 siRNA (10 μL of 50 pmol/μL; GenScript, Wuhan, China) mixed with the Entranster transfection reagent (Engreen Biosystem; Beijing, China) was injected to a 4.5-mm depth below the skull at a rate of 2 μL/min. Rats in the ICH + scramble siRNA group were injected with an equal volume (10 μL) of scramble siRNA into the burr hole. After 24 hours, all rats underwent the procedures for ICH inducement.

After all treatments, rats received food and water ad libitum. After 24 hours, neurological behavior assessments including modified Neurological Severity score (mNSS) and corner turn test were performed. After the neurological function assessment, the rats were sacrificed. The perihematomal tissues were isolated at 2 mm around the hematoma for further experiments. Moreover, brain tissues of rats in each group were serially cut into several sections to evaluate the hematoma area.

Modified Neurological Severity score

Neurological behavior changes were evaluated by mNSS as previously described (Chen et al., 2001). Briefly, the neurological behavior score ranged from 0 to 18 (normal, 0; maximal injury, 18). The mNSS consists of motor tests (maximum = 6), sensory tests (maximum = 2), beam balance tests (maximum = 6), and reflex absence and abnormal movements (maximum = 4). In each of the tests, one point was given for the failure to test or the lack of a tested reflex. Therefore, a higher score indicated a more severe deficit.

Corner turn test

The corner turn test was performed to assess neurological behavior as previously described (Hua et al., 2002). Rats were allowed to enter a corner at a 30° angle, then turned to the left or the right to leave the corner. All tests were recorded. The trials were repeated 12 times with at least 1 minute between the behaviors, and the proportion of right turns (corner turn score) was calculated. Excluding the ventral inversion or horizontal rotation, only turns involving full rearing along either wall were included. The rats were not picked up immediately after each turn so that they did not develop an aversion for their prepotent turning response.

Brain water content

At 24 hours after the neurological behavior assessment, rats were sacrificed with 200 mg/kg sodium pentobarbital by intraperitoneal injection. The skull was removed rapidly, and brain tissues were isolated without the brain stem and divided into five pieces. The pieces were swiftly weighed to obtain the wet weight and then dried at 100°C for 24 hours to obtain the dry weight. The brain water content was calculated as a percentage using the following formula: (wet weight – dry weight)/wet weight × 100.

Fluro-Jade B staining

Fluro-Jade B is a cell death marker that was chosen for demonstration of neuroprotection (Abd-El-Basset and Rao, 2018). At 24 hours after ICH, brain tissue sections were incubated with 1% NaOH (mixed with 80% ethanol) for 5 minutes. Sections were maintained in 70% ethanol for 2 minutes, followed by incubation with 0.06% potassium permanganate for 10 minutes. Slices were transferred to Fluro-Jade B solution (Merck Millipore, Billerica, MA, USA) for 20 minutes and protected from light. After rinsing with distilled water, sections were dried at 50°C for 5 minutes and fixed with neutral balata. Images were captured on a BX53 fluorescence microscope (Olympus, Tokyo, Japan).

Quantitative reverse transcription-polymerase chain reaction

OLR1 mRNA expression was detected using quantitative reverse transcription-polymerase chain reaction (qRT-PCR) at 24 hours after ICH. Total RNA was extracted from rat brain tissues around hematoma with the TRIpure kit (BioTek Instruments, Winooski, VT, USA) in accordance with the manufacturer's protocols. Reverse transcription of RNA to complementary DNA was performed using BeyoRT II M-MLV reverse transcriptase (Beyotime, Shanghai, China). PCR was performed with the 2× Taq PCR MasterMix (Solarbio, Shanghai, China) and SYBR Green (Solarbio) in accordance with the manufacturer's instructions. For normalization of gene expression, *β-actin* mRNA was used as an internal control. Primers were synthesized by GenScript, and the sequences are as follows: *OLR1* forward: 5′-CCT GCT GTG ACT CTG-3′; reverse: 5′-TTC CCT CTT TGA TTC TTG TG-3′. *β-Actin* forward: 5′-GGA GAT TAC TGC CCT GGC TCC TAG C-3′; reverse: 5′-GGC CGG ACT CAT CGT ACT CCT GCT T-3′. The program was as follows: 94 °C for 5 minutes, 94°C for 20 seconds, 60°C for 30 seconds, 72°C for 40 seconds; 40 cycles of 72°C for 5.5 minutes and 40°C for 4.5 minutes; and finally 25°C for 1–2 minutes. Data were analyzed using the $2^{-\Delta\Delta CT}$ method.

Western blot analysis

At 24 hours after ICH, total protein was extracted from rat brain tissues around hematoma using protein lysis buffer (Beyotime) containing 1% phenylmethanesulfonyl fluoride. Protein concentration was measured using the Enhanced Bicinchoninic Acid Assay Kit (Beyotime) following the manufacturer's protocols. Protein samples were separated by sodium dodecyl sulfate polyacrylamide gel electrophoresis and then transferred to polyvinylidene fluoride membranes (Thermo Fisher Scientific, Pittsburgh, PA, USA). After

blocking with 5% bovine serum albumin (Biosharp Life Science, Hefei, China), the membrane was incubated with primary antibodies at 4°C overnight, followed by incubation with horseradish-peroxidase (HRP)-conjugated goat anti-rabbit IgG (1:10,000; RRID: AB_2722564; Cat# SA00001-2, Proteintech, Wuhan, China) or HRP-conjugated goat anti-mouse IgG (1:10,000; RRID: AB_2722565; Cat# SA00001-1, Proteintech) at 37°C for 40 minutes.

The primary antibodies are listed as follows: rabbit polyclonal anti-OLR1 (1:1000; RRID: AB_2763697; Cat# A1639; ABclonal Technology, Shanghai, China), rabbit polyclonal anti-COX-2 (ferroptosis marker; 1:500; RRID: AB_2759370; Cat# A1253, ABclonal Technology), rabbit polyclonal anti-GPX4 (ferroptosis marker; 1:500; RRID: AB_2763960; Cat# A1933, ABclonal Technology), rabbit polyclonal anti-ferritin heavy polypeptide 1 (FTH1; ferroptosis marker; 1:500; RRID: AB_2862659; Cat# A19544, ABclonal Technology), rabbit polyclonal anti-p-p38 (1:500; RRID: AB_2771309; Cat# AP0526, ABclonal Technology), rabbit polyclonal p38 (1:500; RRID: AB_2761271; Cat# A14401, ABclonal Technology), and mouse monoclonal β-actin (1:2000; RRID: AB_2289225; Cat# 60008-1-Ig, Proteintech).

Membranes were washed with Tris-buffered saline plus Tween-20 and then treated with Immobilon western HRP substrate solution (7 Sea Biotech, Shanghai, China). Images were scanned by a WD-9413 gel imager (Liuyi Biotech, Beijing, China). The optical density of bands was analyzed using Gel-Pro-Analyzer software (Media Cybernetics, Bethesda, MD, USA).

Enzyme-linked immunosorbent assay

At 24 hours after ICH, rat brain tissues around hematoma and saline at 1:9 (g/mL) were homogenized and the samples were centrifuged at 421 × *g* for 10 minutes. The supernatant was used for detecting the concentration of interleukin-1β (IL-1β), interleukin-6 (IL-6), tumor necrosis factor-α (TNF-α), and 4-hydroxynonenal (4-HNE) using the IL-1β enzyme-linked immunosorbent assay (ELISA) kit, IL-6 ELISA kit, TNF-α ELISA kit, and 4-HNE ELISA kit purchased from Nanjing Jiancheng Bioengineering Institute (Nanjing, China) following the manufacturer's instructions.

Immunofluorescence staining

Paraffin-embedded sections of the brain tissues around hematoma (5 μm) were deparaffinized in xylene and rehydrated in an ethanol gradient with distilled water. Antigen retrieval of brain tissues sections was performed in a pressure cooker for 5 minutes and the sections were blocked with goat serum (Solarbio) for 15 minutes at room temperature. The sections were then incubated with the following primary antibodies: rabbit polyclonal anti-myeloperoxidase (MPO; neutrophil marker; RRID: AB_2760599; Cat# A1374, 1:100; ABclonal Technology), mouse monoclonal anti-NeuN (neuronal nuclei biomarker (Duan et al., 2016); 1:300; RRID: AB_10711040; Cat# ab104224, Abcam, Cambridge, UK), rabbit polyclonal anti-GPX4 (1:100; RRID: AB_2763960; Cat# A1933, ABclonal Technology), rabbit polyclonal anti-glial fibrillary acidic protein (GFAP; astrocyte marker; 1:100; RRID: AB_2893014; Cat# WL0836, Wanleibio, Shenyang, China), and rabbit monoclonal anti-ionized calcium-binding adaptor molecule 1 (Iba1; microglia/macrophage marker; 1:100; RRID: AB_2832244; Cat# ab178847, Abcam) at 4°C overnight. Samples were washed three times with phosphate buffer saline, followed by incubation with Cy3-conjugated goat anti-rabbit IgG (1:200; RRID: AB_2893015; Cat# A0516, Beyotime) or fluorescein isothiocyanate-conjugated goat anti-mouse IgG (1:200; RRID: AB_2893016; Cat# A0568, Beyotime) at room temperature for 90 minutes in the dark. Sections (except for the GAFP- and Iba1-stained sections) were further counterstained with 2-(4-amidinophenyl)-6-indolecarbamidine dihydrochloride (Aladdin, Shanghai, China). Photographs were taken using a BX53 fluorescence microscope.

Evaluation of reactive oxygen species formation

Superoxide production was assessed by fluorescent-labeled dihydroethidium staining at 24 hours after ICH. Rat brain sections around hematoma were incubated with dihydroethidium (1:100; Beyotime) at 37°C for 30 minutes protected from the light. The images were captured using a BX53 fluorescence microscope.

Determination of superoxide dismutase, glutathione, and malondialdehyde levels

Rat brain tissues around hematoma were isolated and homogenized with saline at 1:9 (g/mL), and the samples were centrifuged at 421 × *g* for 10 minutes. The supernatant was used for the determination of global superoxide dismutase (SOD), GSH, and MDA levels using the SOD test kit, GSH assay kit, and MDA test kit, respectively, purchased from Nanjing Jiancheng Bioengineering Institute, in accordance with the manufacturer's instructions.

Statistical analysis

The selected sample size was calculated by power analysis using G*power 3.1.9.7 software (https://www.psychologie.hhu.de/arbeitsgruppen/allgemeine-psychologie-und-arbeitspsychologie/gpower.html) with n = 24, power = 0.86, and α error probe = 0.05. The evaluators were blind to the groups for the assessment of neurological behavior. Statistical analysis was performed using GraphPad Prism 8.0 software (GraphPad Software, La Jolla, CA, USA). Data are presented as mean ± standard deviation (SD) except for the boxplot (median, interquartile range, maximum and minimum). The difference among four groups was analyzed using one-way analysis of variance following by Bonferroni's *post hoc* test. Neurological function results were analyzed by nonparametric tests (Kruskal-Wallis, followed by Dunn's *post hoc* test). Six independent repeats were performed in each experiment except for the neurological function assessment (twelve independent repeats). $P < 0.05$ was considered statistically significant.

Results

Silencing *OLR1* attenuates neurological behavior impairment, hematoma expansion, brain water content, and neuron loss in rat brain tissues after ICH

To investigate the role of OLR1 in the functional impairment after ICH, we established ICH model rats as described in Methods and evaluated the effects of *OLR1* knockdown on neurological behavioral changes after ICH. As shown in **Figure 1A** and **B**, ICH-mediated induction of OLR1 mRNA and protein levels was decreased by the downregulation of *OLR* in brain tissues after ICH. Knockdown of *OLR1* recovered the neurological dysfunction after ICH, as evidenced by the reverse of the ICH-mediated increase in mNSS score and corner turn score (**Figure 1C** and **D**). Furthermore, knockdown of *OLR1* decreased the elevated brain water content and the increased hematoma area of serial brain sections of rats caused by ICH (**Figure 1E** and **F**). Moreover, downregulation of *OLR1* reverted the ICH-induced neuron loss of brain tissues, as shown by Fluro-Jade B staining (**Figure 1G**). Together, these results indicated that decreased expression of *OLR1* attenuated the functional impairment, hematoma expansion, brain water content, and neuron loss in brain tissues post-ICH.

Silencing of *OLR1* alleviates the inflammation of rat brain tissues after intracerebral hemorrhage

To determine the contribution of OLR1 to inflammation, we examined the secretion of pro-inflammatory factors using ELISA. The results revealed that silencing of OLR1 reduced the increased concentration of IL-1β, IL-6, and TNF-α in the supernatant of rat brain tissues after ICH (**Figure 2A–C**).

We next examined the infiltration of immunocytes in brain tissues by immunofluorescence staining for indicators of neutrophils, microglia/macrophages, and astrocytes (MPO, Iba1, and GFAP, respectively). As shown in **Figure 2D**, OLR1 knockdown reversed the elevated MPO in brain tissues induced by ICH. The same findings were observed for Iba1 and GFAP levels (**Additional Figure 1**). These results suggested that *OLR1* knockdown alleviated the inflammation of brain tissues around hematoma after ICH.

Silencing of *OLR1* mitigates oxidative stress in rat brain tissues after intracerebral hemorrhage

We further investigated the effects of *OLR1* on oxidative stress, which plays an important function in mediating ICH-induced injury and is characterized by the gain of ROS, MDA, 4-HNE and the loss of SOD and GSH. Dihydroethidium fluorescence assay demonstrated that the knockdown of OLR1 reversed the increased ROS in post-ICH brain tissues (**Figure 3A**). Furthermore, downregulation of OLR1 partially restored the reduced global SOD activity and GSH content and reversed the enhanced MDA and 4-HNE in the supernatant of rat brain tissues after ICH (**Figure 3B–E**). These data indicated that silencing of *OLR1* mitigated oxidative stress in rat brain tissues after ICH.

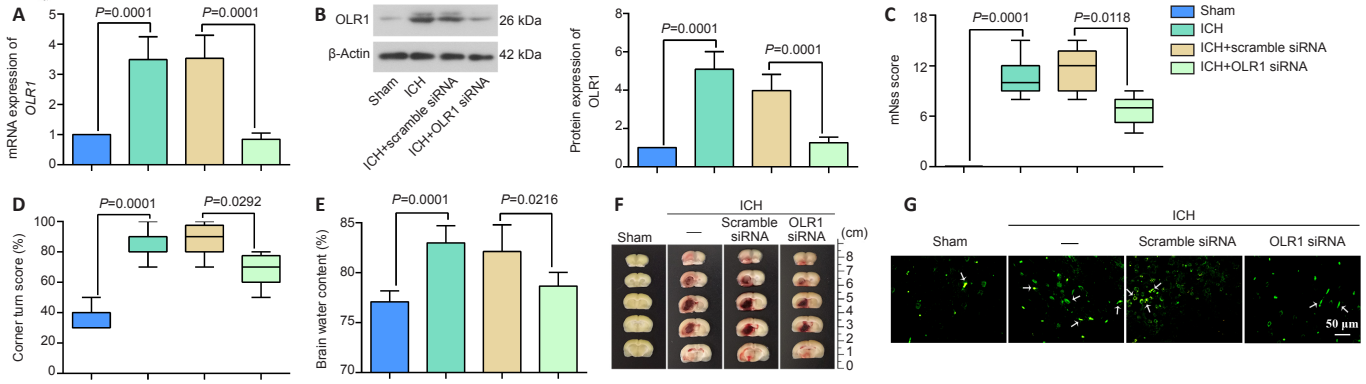

Figure 1 | **Silencing *OLR1* attenuates functional impairment, hematoma expansion, brain water content, and neuron loss in rat brain tissues 24 hours after ICH.**

After injection with *OLR1* siRNA or scramble siRNA for 24 hours, rats were infused with collagenase type VII to induce ICH. (A, B) The mRNA (A) and protein (B) levels of OLR1 by quantitative reverse transcription-polymerase and western blot analysis. (C) mNSS score. A higher score was accompanied with severe deficit. (D) Corner turn score. (E) Brain water content. (F) Representative images of brain sections. Depletion of OLR1 decreased the increased hematoma area in serial brain sections of rats after ICH. (G) Fluro-Jade B-stained cells. The downregulation of OLR1 reverted the ICH-induced neuron loss of brain tissues. White arrows indicate neuron loss. Scale bar: 50 μm. Data in A, B and E are shown as mean ± SD (n = 6) and were analyzed by one-way analysis of variance following by Bonferroni's *post hoc* test. Data in C and D are shown as median, interquartile range, maximum and minimum and were analyzed by Kruskal-Wallis test followed by Dunn's *post hoc* test. The experiments were repeated 12 times in C and D, and six times in other figures. ICH: Intracerebral hemorrhage; mNss: modified Neurological Severity score; OLR1: oxidized low-density lipoprotein receptor 1; siRNA: small interfering RNA.

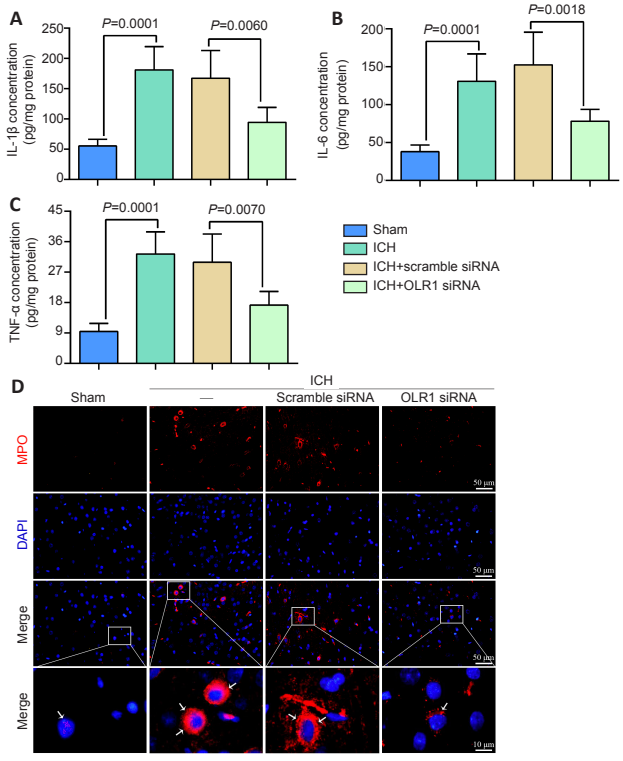

Figure 2 | **Silencing of *OLR1* alleviates the inflammation of rat brain tissues 24 hours after ICH.**

After injection with *OLR1* siRNA or scramble siRNA for 24 hours, rats were infused with collagenase type VII to induce ICH. (A–C) Concentrations of IL-1β, IL-6 and TNF-α in the supernatant of rat brain tissues as detected by enzyme-linked immunosorbent assay. (D) Representative immunofluorescence staining to identify MPO-positive cells. The loss of OLR1 reversed the elevated MPO in brain tissues induced by ICH. MPO-positive cells (white arrows) were labeled red with Cy3. Nuclei were labeled blue by DAPI. Scale bar: 50 μm (top three rows), 10 μm (bottom row). Data are shown as mean ± SD and were analyzed by one-way analysis of variance following by Bonferroni's *post hoc* test. The experiments were repeated six times. DAPI: 2-(4-Amidinophenyl)-6-indolecarbamidine dihydrochloride; ICH: intracerebral hemorrhage; IL: interleukin; MPO: myeloperoxidase; OLR1: oxidized low-density lipoprotein receptor 1; siRNA: small interfering RNA; TNF-α: tumor necrosis factor-α.

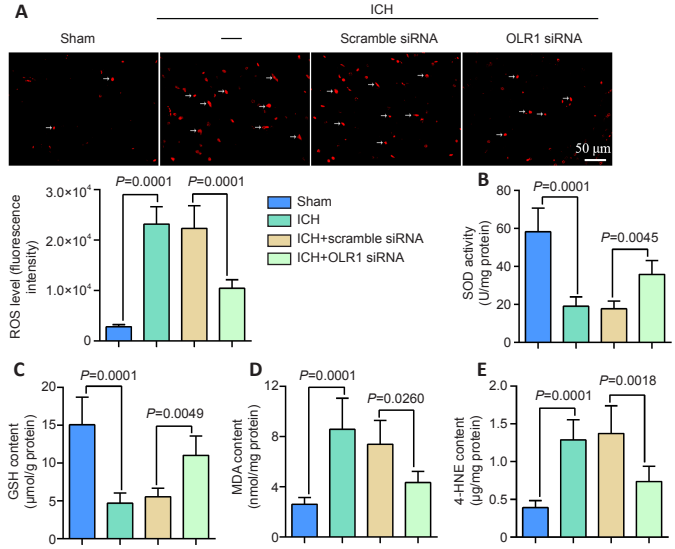

Figure 3 | **Silencing of *OLR1* mitigates oxidative stress in rat brain tissues after ICH.**

After injection with *OLR1* siRNA or scramble siRNA for 24 hours, rats were infused with collagenase type VII to induce ICH. (A) Representative staining with dihydroethidium (a fluorescent ROS indicator; indicated by white arrows). The loss of OLR1 rescued the increased ROS levels in brain tissues induced by ICH. Scale bar: 50 μm. (B) SOD activity. (C–E) Contents of GSH, MDA, and 4-HNE. Data are shown as mean ± SD (n = 6) and were analyzed by one-way analysis of variance followed by Bonferroni's *post hoc* test. The experiments were repeated six times. GSH: Glutathione; ICH: intracerebral hemorrhage; MDA: malondialdehyde; OLR1: oxidized low-density lipoprotein receptor 1; siRNA: small interfering RNA; ROS: reactive oxygen species; SOD: superoxide dismutase; 4-HNE: 4-hydroxynonenal.

Silencing of *OLR1* suppresses ferroptosis of neuron in rat brain tissues after intracerebral hemorrhage

We next investigated the mechanism underlying the effects of *OLR1* knockdown after ICH. GSH depletion reduces GPX4 activity and cell antioxidant capacity, resulting in the accumulation of lipid ROS and ultimately the occurrence of oxidative damage and ferroptosis (Wang et al., 2019; Li et al., 2020). Given the data on the impact of OLR1 on GSH and oxidative stress, we speculated that the loss of OLR1 might prevent secondary brain injury in ICH rats by regulating ferroptosis. We thus next examined protein expression levels of ferroptotic indicators (GPX4, FTH1, and COX-2) (Datta et al., 2013; Chen et al., 2019; Seibt et al., 2019). Western blot analysis showed that *OLR1* depletion reversed the downregulation of GPX4 and FTH1 and the upregulation of COX-2 in brain tissues around hematoma after ICH (**Figure 4A**). Moreover, immunofluorescence staining results of GPX4 expression in NeuN-positive cells showed similar results; GPX4 was localized in cytoplasm (**Figure 4B**). These results indicated that silencing of *OLR1* suppressed the ferroptosis of neurons in rat brain tissues induced by ICH.

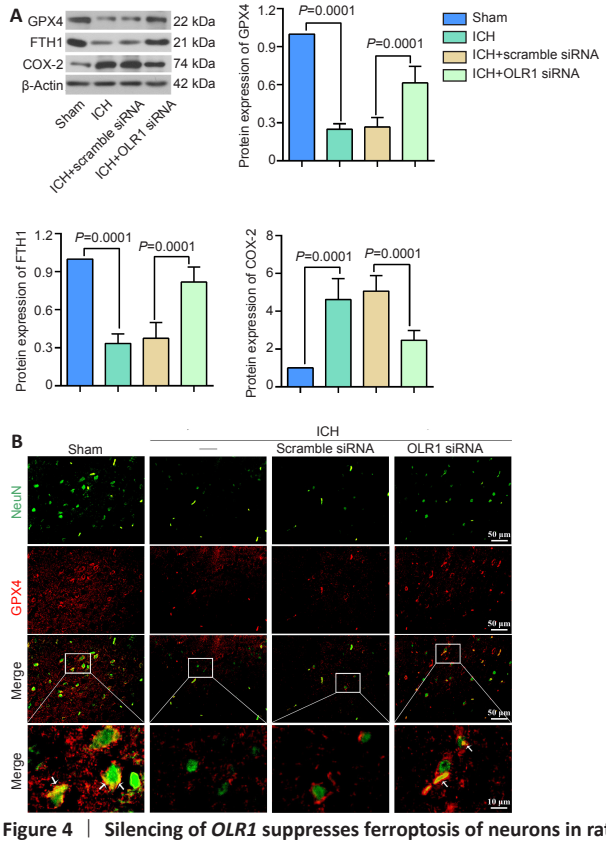

Figure 4 | Silencing of *OLR1* suppresses ferroptosis of neurons in rat brain tissues 24 hours after ICH.

After injection with *OLR1* siRNA or scramble siRNA for 24 hours, rats were infused with collagenase type VII to induce ICH. (A) Protein expression of GPX4, FTH1, and COX-2. Protein expression was normalized by levels in the sham group. (B) Representative immunofluorescence staining with NeuN and GPX4. Knockdown of OLR1 reversed the ICH-induced decrease of GPX4 levels in NeuN-positive cells. NeuN-positive cells were labeled by FITC (green), and GPX-4-positive cells were labeled by Cy3 (red). White arrows indicate the NeuN-positive cells with GPX4 expression. Scale bar: 50 μm (upper three rows), 10 μm (lower row). Data are shown as mean ± SD (n = 6) and are analyzed by one-way analysis of variance followed by Bonferroni's *post hoc* test. COX-2: Cyclooxygenase-2; FITC: fluorescein Isothiocyanate; FTH1: ferritin heavy polypeptide 1; GPX4: glutathione peroxidase 4; ICH: intracerebral hemorrhage; OLR1: oxidized low-density lipoprotein receptor 1; siRNA: small interfering RNA.

Silencing of *OLR1* represses the p38 signaling pathway in brain tissues after intracerebral hemorrhage

Studies have shown that downregulated GPX4-triggered ferroptosis is mediated by p38 activation (Zhang et al., 2020c; Wang et al., 2021). To get a deeper understanding of the mechanism of OLR1 in regulating ferroptosis after ICH, we examined the effects of *OLR1* knockdown on p38 activation. As shown in **Figure 5**, the knockdown of *OLR1* partially reversed ICH-mediated activation of p38.

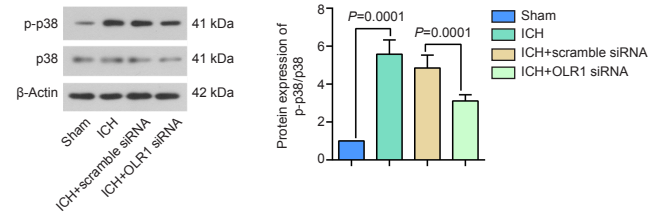

Figure 5 | Silencing of *OLR1* represses the p38 signaling pathway 24 hours after ICH.

The protein levels of p-p38 and p38 were evaluated in brain tissues of rats injected with *OLR1* siRNA or scramble siRNA, followed by infusion with collagenase type VII to induce ICH. Data are shown as mean ± SD (n = 6) and are analyzed by one-way analysis of variance following by Bonferroni's *post hoc* test. The experiments were repeated six times. ICH: Intracerebral hemorrhage; OLR1: oxidized low-density lipoprotein receptor 1; siRNA: small interfering RNA.

Together, these results indicate that *OLR1* silencing protected the post-ICH brain tissues from secondary brain injury by the inhibition of ferroptosis, which might be mediated by the p38 signaling pathway (**Additional Figure 2**).

Discussion

ICH is a fatal cerebral disease with high morbidity and mortality rates (Hostettler et al., 2019). Increasing evidence has suggested that brain damage induced by the occurrence of intraparenchymal blood causes oxidative stress, overproduction of ROS, and brain edema, which ultimately lead to cerebral injury and neurological deterioration (Zhou et al., 2014; Wilkinson et al., 2018). Thus, amelioration of these brain injuries is of great significance for the treatment of ICH. Previous studies showed that amelioration of ICH-induced secondary brain injury is mediated by the suppression of inflammation, oxidative stress, and mitochondria and DNA damage (Wang et al., 2018; Yang et al., 2021). In this work, we found that knockdown of *OLR1* attenuated the neurological behavior impairment, hematoma expansion, brain water content and neuron loss in rat brain tissues induced by ICH. Furthermore, downregulation of *OLR1* alleviated inflammation and oxidative stress in post-ICH brain tissues. Moreover, the protective effects of *OLR1* silencing on ICH-induced cerebral damage may be mediated by inhibition of neuronal ferroptosis and repression of the p38 signaling pathway.

OLR1 is a type II single-pass transmembrane glycoprotein and the receptor for oxidized low-density lipoprotein (Jiang et al., 2019). OLR1 has been implicated in the progression of various diseases, such as atherosclerosis, diabetes mellitus, ischemia/reperfusion cerebral injury, gastric cancer, and osteoarthritis (Hashimoto et al., 2016; Li et al., 2017; Akhmedov et al., 2019; Stankova et al., 2019; Takemura et al., 2019). A previous study showed that the serum OLR1 levels of ICH patients are significantly higher than that of healthy individuals, indicating the potential role for OLR1 as a biomarker of ICH (Inoue et al., 2019). Liang et al. (2020) reported that knockdown of OLR1 attenuates spontaneous brain damage in stroke-pone hypertensive rats. Yuan et al. (2020) demonstrated that the neuroprotective effect in ischemic stroke (the alleviation of brain water content and neurological outcome) from the downregulation of *OLR1* is mediated by the inhibition of inflammation (secretion of IL-1β, IL-6, and TNF-α), SOD, GSH, and catalase via the suppression of NF-κB signaling. Ge et al. (2019) showed that OLR1 facilitates microglia activation and aggravates neuroinflammation-induced neuronal apoptosis and neuronal injury. These studies indicate the potential role of OLR1 in cerebral diseases. In the current study, we found that loss of *OLR1* partially reversed the changes in functional impairment, hematoma expansion, brain water content, and neuron loss in rat brain tissues after ICH. Silencing of *OLR1* reversed the increased inflammation as reflected by changes in IL-1β, IL-6, TNF-α, and MPO in brain tissues following ICH. The aggravated oxidative stress was reversed by the downregulation of *OLR1* with changes in ROS, MDA, 4-HNE, SOD and GSH in post-ICH brain tissues.

The accumulation of iron released from hematoma after ICH may be a contributor of oxidative stress and perihematomal edema and causes ferroptosis (Zhou et al., 2020). Ferroptosis is characterized by GSH antioxidant dysfunction, GPX4 depletion, the accumulation of lipid hydroperoxides, and ROS overproduction (Ren et al., 2020b; Zhou et al., 2020). Research has shown that suppression of ferroptotic cell death might markedly prevent secondary brain injury after ICH (Zhang et al., 2018; Chen et al., 2019; Bai et al., 2020). Duan et al. (2021) reported that ferroptosis depletion protects ICH-induced brain tissues from motor deficits, hematoma expansion, iron deposition, and neuronal degradation by upregulating GPX4, solute carrier family 11 membrane 7, and reducing ROS levels. Guo et al. (2017) demonstrated that aortic atherosclerosis lesions are abrogated via the decreased levels of blood lipid and MDA as well as the enhanced content of GSH and SOD. These effects were mediated by downregulating the expression of OLR1 and the oxidized low-density lipoprotein. Therefore, interventions targeting ferroptosis may represent a potential strategy in the therapy of various diseases. In this study, we found that downregulation of OLR1 expression repressed the ICH-induced ferroptosis of neurons by reversing ICH-mediated downregulation of GPX4 and FTH1 and upregulation of COX-2. OLR1 repression ameliorates Ang II-induced oxidant stress and the relative levels of nicotinamide adenine dinucleotide phosphate (NADPH) oxidase (a membrane-bound enzyme complex) (Lu et al., 2011). ROS generated by NAPDH oxidase induces lipid peroxidation by reacting with the polyunsaturated fatty acids of lipid membranes,

resulting in ferroptosis (Ma et al., 2017; Hou et al., 2019). Zhang et al. (2014) found that either genetic loss or pharmacological suppression of NAPDH oxidase mitigates ROS overproduction and lipid peroxidation in pathological progression of various diseases. On the basis of these results and combined with the findings of the inhibitory effects of depleted *OLR1* on ROS levels in the current study, we speculate that *OLR1* downregulation might block ROS production by decreasing NADPH oxidase levels, leading to the attenuation of lipid peroxidation and ferroptosis.

p38 is a mitogen-activated protein kinase (MAPK) that responds to stimulation by regulating cell proliferation, apoptosis, ferroptotic cell death, oxidative stress, and inflammation (Son et al., 2013; Wei and Hsieh, 2020). In coronary syndrome, knockdown of *OLR1* enhances vascular remodeling and inhibits the secretion of the inflammatory response-related factors by repressing the p38 MAPK pathway (Yu et al., 2020). Depleted *OLR1* influences autophagy via reducing NADPH oxidase in the brain tissues of hypertensive rats by weakening the p38 MAPK pathway (Ding et al., 2015). The OLR1/p38-MAPKs/NF-κB positive feedback loop may facilitate microglia activation and aggravate neuroinflammation and neuronal injury (Ge et al., 2019). These findings indicate that *OLR1* plays an essential part in the progression of cerebral diseases and vascular diseases through regulation of the p38 signaling pathway. In this study, we found that downregulation of *OLR1* restored the upregulation of p-p38 in post-ICH brain tissues of rat, suggesting that the brain protective function triggered by *OLR1* in ICH involves the p38 pathway.

Ferroptosis is regulated by the activation of p38 MAPK. p38-mediated GPX4 downregulation has been reported to participate in ferroptosis in the progression of endometrial cancer, and ROS-dependent p38 activation is a robust activator of ferroptosis and apoptosis that inhibits the development of hepatocellular carcinoma (Chang et al., 2021; Wang et al., 2021). Li et al. (2018) showed that suppression of the p38 MAPK activation blocks ferroptotic cell death triggered by deprivation/reoxygenation. A ferroptotic inhibitor alleviated the cognitive impairment of epileptic rats through the regulation of synaptic protein by repressing the p38 MAPK pathway (Ye et al., 2020). Furthermore, *LOX-1* knockout mice exhibit reduced myocardial ischemia/reperfusion injury and decreased levels of p38 (Hu et al., 2008). These studies suggest that the p38 MAPK pathway participates in the regulation of ferroptosis in various diseases. On the basis of our results showing that *OLR1* silencing regulates p38 activation, we considered that the *OLR1* downregulation–induced ferroptotic attenuation might be mediated by the suppression of p38 activation. We speculate that knockdown of *OLR1* inhibited p38 MAPK signaling, which further repressed ferroptosis, as evidenced by the upregulation of GPX4 and the downregulation of COX-2. The suppression of ferroptosis further resulted in the mitigation of inflammation, as evidenced by the downregulation of MPO.

This study has several limitations. First, the collagenase type VII-induced rat model of ICH does not completely simulate the pathological characteristics of ICH patients. Second, we found that *OLR1* knockdown protected against ICH via regulating ferroptosis by repressing the p38 signaling pathway. However, the mechanism by which blocking p38 improves ICH outcome has not been studied. Future investigations should address these issues.

In conclusion, our results show that *OLR1* silencing ameliorated secondary brain injury in ICH through blocking of ferroptosis by inhibiting the p38 signaling pathway. These findings suggest that *OLR1* might be a novel target of ICH therapy.

Author contributions: *Study conception: HYZ, ZYH; study design: HYZ, XL, LT, YHH, ZYH; experimental implementation: HYZ, XL; data analysis: HYZ, LT, YHH; statistical analysis: HYZ, XL, LT; manuscript preparation: HYZ; manuscript revision: ZYH. All authors approved the final manuscript before submission for publication.*
Conflicts of interest: *The authors declare that there are no conflicts of interest associated with this manuscript.*
Availability of data and materials: *All data generated or analyzed during this study are included in this published article and its supplementary information files.*

Open peer reviewer: *Rosario Donato, Universita degli Studi di Perugia, Italy.*
Additional files:
Additional Figure 1: *Representative immunofluorescence staining to identify GFAP- or Iba1-positive cells.*
Additional Figure 2: *The mechanism graph of OLR1/p38 axis and ferroptosis involves in the protective effects of ICH.*
Additional file 1: *Open peer review report 1.*

References

Abd-El-Basset EM, Rao MS (2018) Dibutyryl cyclic adenosine monophosphate rescues the neurons from degeneration in stab wound and excitotoxic injury models. Front Neurosci 12:546.

Akhmedov A, Sawamura T, Chen CH, Kraler S, Vdovenko D, Lüscher TF (2021) Lectin-like oxidized low-density lipoprotein receptor-1 (LOX-1): a crucial driver of atherosclerotic cardiovascular disease. Eur Heart J 42:1797-1807.

Akhmedov A, Bonetti NR, Reiner MF, Spescha RD, Amstalden H, Merlini M, Gaul DS, Diaz-Cañestro C, Briand-Schumacher S, Spescha RS, Semerano A, Giacalone G, Savarese G, Montecucco F, Kulic L, Nitsch RM, Matter CM, Kullak-Ublick GA, Sessa M, Lüscher TF, et al. (2019) Deleterious role of endothelial lectin-like oxidized low-density lipoprotein receptor-1 in ischaemia/reperfusion cerebral injury. J Cereb Blood Flow Metab 39:2233-2245.

Bai Q, Liu J, Wang G (2020) Ferroptosis, a regulated neuronal cell death type after intracerebral hemorrhage. Front Cell Neurosci 14:591874.

Bai Y, Meng L, Han L, Jia Y, Zhao Y, Gao H, Kang R, Wang X, Tang D, Dai E (2019) Lipid storage and lipophagy regulates ferroptosis. Biochem Biophys Res Commun 508:997-1003.

Bao WD, Zhou XT, Zhou LT, Wang F, Yin X, Lu Y, Zhu LQ, Liu D (2020) Targeting miR-124/Ferroportin signaling ameliorated neuronal cell death through inhibiting apoptosis and ferroptosis in aged intracerebral hemorrhage murine model. Aging Cell 19:e13235.

Barreto J, Karathanasis SK, Remaley A, Sposito AC (2021) Role of LOX-1 (lectin-like oxidized low-density lipoprotein receptor 1) as a cardiovascular risk predictor: mechanistic insight and potential clinical use. Arterioscler Thromb Vasc Biol 41:153-166.

Chang WT, Bow YD, Fu PJ, Li CY, Wu CY, Chang YH, Teng YN, Li RN, Lu MC, Liu YC, Chiu CC (2021) A marine terpenoid, heteronemin, induces both the apoptosis and ferroptosis of hepatocellular carcinoma cells and involves the ROS and MAPK pathways. Oxid Med Cell Longev 2021:7689045.

Chen B, Chen Z, Liu M, Gao X, Cheng Y, Wei Y, Wu Z, Cui D, Shang H (2019) Inhibition of neuronal ferroptosis in the acute phase of intracerebral hemorrhage shows long-term cerebroprotective effects. Brain Res Bull 153:122-132.

Chen J, Sanberg PR, Li Y, Wang L, Lu M, Willing AE, Sanchez-Ramos J, Chopp M (2001) Intravenous administration of human umbilical cord blood reduces behavioral deficits after stroke in rats. Stroke 32:2682-2688.

Chen S, Yang Q, Chen G, Zhang JH (2015) An update on inflammation in the acute phase of intracerebral hemorrhage. Transl Stroke Res 6:4-8.

Datta A, Akatsu H, Heese K, Sze SK (2013) Quantitative clinical proteomic study of autopsied human infarcted brain specimens to elucidate the deregulated pathways in ischemic stroke pathology. J Proteomics 91:556-568.

Deng H, Zhang Y, Li GG, Yu HH, Bai S, Guo GY, Guo WL, Ma Y, Wang JH, Liu N, Pan C, Tang ZP (2021) P2X7 receptor activation aggravates NADPH oxidase 2-induced oxidative stress after intracerebral hemorrhage. Neural Regen Res 16:1582-1591.

Ding Z, Liu S, Wang X, Khaidakov M, Fan Y, Deng X, Xiang D, Mehta JL (2015) Lectin-like oxidized low-density lipoprotein receptor-1 regulates autophagy and Toll-like receptor 4 in the brain of hypertensive mice. J Hypertens 33:525-533; discussion 533.

Djulbegovic MB, Uversky VN (2019) Ferroptosis- an iron- and disorder-dependent programmed cell death. Int J Biol Macromol 135:1052-1069.

Duan L, Zhang Y, Yang Y, Su S, Zhou L, Lo PC, Cai J, Qiao Y, Li M, Huang S, Wang H, Mo Y, Wang Q (2021) Baicalin inhibits ferroptosis in intracerebral hemorrhage. Front Pharmacol 12:629379.

Duan W, Zhang YP, Hou Z, Huang C, Zhu H, Zhang CQ, Yin Q (2016) Novel insights into neun: from neuronal marker to splicing regulator. Mol Neurobiol 53:1637-1647.

Fan BY, Pang YL, Li WX, Zhao CX, Zhang Y, Wang X, Ning GZ, Kong XH, Liu C, Yao X, Feng SQ (2021) Liproxstatin-1 is an effective inhibitor of oligodendrocyte ferroptosis induced by inhibition of glutathione peroxidase 4. Neural Regen Res 16:561-566.

Feng H, Stockwell BR (2018) Unsolved mysteries: How does lipid peroxidation cause ferroptosis? PLoS Biol 16:e2006203.

Ge X, Zhang DM, Li MM, Zhang Y, Zhu XY, Zhou Y, Peng X, Shen AG (2019) Microglial LOX-1/MAPKs/NF-κB positive loop promotes the vicious cycle of neuroinflammation and neural injury. Int Immunopharmacol 70:187-200.

Guo JE, Mi SB, Yan XC, Xin SY, Gao F, Liang GH, Li JH (2017) Effects of Gualou Xiebai Banxia decoction on blood lipid content, oxidative stress and ox-LDL/Lox-1 pathway in ApoE$^{-/-}$ mice. Zhongguo Zhong Yao Za Zhi 42:752-757.

Hashimoto K, Mori S, Oda Y, Nakano A, Sawamura T, Akagi M (2016) Lectin-like oxidized low density lipoprotein receptor 1-deficient mice show resistance to instability-induced osteoarthritis. Scand J Rheumatol 45:412-422.

Hostettler IC, Seiffge DJ, Werring DJ (2019) Intracerebral hemorrhage: an update on diagnosis and treatment. Expert Rev Neurother 19:679-694.

Hou L, Huang R, Sun F, Zhang L, Wang Q (2019) NADPH oxidase regulates paraquat and maneb-induced dopaminergic neurodegeneration through ferroptosis. Toxicology 417:64-73.

Hu C, Chen J, Dandapat A, Fujita Y, Inoue N, Kawase Y, Jishage K, Suzuki H, Li D, Hermonat PL, Sawamura T, Mehta JL (2008) LOX-1 abrogation reduces myocardial ischemia-reperfusion injury in mice. J Mol Cell Cardiol 44:76-83.

Hua Y, Schallert T, Keep RF, Wu J, Hoff JT, Xi G (2002) Behavioral tests after intracerebral hemorrhage in the rat. Stroke 33:2478-2484.

Inoue T, Ishida T, Inoue T, Saito A, Ezura M, Uenohara H, Fujimura M, Sato K, Endo T, Omodaka S, Endo H, Niizuma K, Tominaga T (2019) Lectin-like oxidized low-density lipoprotein receptor-1 levels as a biomarker of acute intracerebral hemorrhage. J Stroke Cerebrovasc Dis 28:490-494.

Jiang L, Jiang S, Zhou W, Huang J, Lin Y, Long H, Luo Q (2019) Oxidized low density lipoprotein receptor 1 promotes lung metastases of osteosarcomas through regulating the epithelial-mesenchymal transition. J Transl Med 17:369.

Li C, Zhang J, Wu H, Li L, Yang C, Song S, Peng P, Shao M, Zhang M, Zhao J, Zhao R, Wu W, Ruan Y, Wang L, Gu J (2017) Lectin-like oxidized low-density lipoprotein receptor-1 facilitates metastasis of gastric cancer through driving epithelial-mesenchymal transition and PI3K/Akt/GSK3β activation. Sci Rep 7:45275.

Li J, Cao F, Yin HL, Huang ZJ, Lin ZT, Mao N, Sun B, Wang G (2020) Ferroptosis: past, present and future. Cell Death Dis 11:88.

Li L, Hao Y, Zhao Y, Wang H, Zhao X, Jiang Y, Gao F (2018) Ferroptosis is associated with oxygen-glucose deprivation/reoxygenation-induced Sertoli cell death. Int J Mol Med 41:3051-3062.

Li Y, Duan Z, Gao D, Huang S, Yuan H, Niu X (2012) The new role of LOX-1 in hypertension induced neuronal apoptosis. Biochem Biophys Res Commun 425:735-740.

Liang YQ, Kakino A, Matsuzaka Y, Mashimo T, Isono M, Akamatsu T, Shimizu H, Tajima M, Kaneko T, Li L, Takeuchi F, Sawamura T, Kato N (2020) LOX-1 (lectin-like oxidized low-density lipoprotein receptor-1) deletion has protective effects on stroke in the genetic background of stroke-prone spontaneously hypertensive rat. Stroke 51:1835-1843.

Liu Z, Zhang R, Chen X, Yao P, Yan T, Liu W, Yao J, Sokhatskii A, Gareev I, Zhao S (2019) Identification of hub genes and small-molecule compounds related to intracerebral hemorrhage with bioinformatics analysis. PeerJ 7:e7782.

Lu J, Mitra S, Wang X, Khaidakov M, Mehta JL (2011) Oxidative stress and lectin-like ox-LDL-receptor LOX-1 in atherogenesis and tumorigenesis. Antioxid Redox Signal 15:2301-2333.

Ma MW, Wang J, Zhang Q, Wang R, Dhandapani KM, Vadlamudi RK, Brann DW (2017) NADPH oxidase in brain injury and neurodegenerative disorders. Mol Neurodegener 12:7.

Ouyang Y, Li D, Wang H, Wan Z, Luo Q, Zhong Y, Yin M, Qing Z, Li Z, Bao B, Chen Z, Yin X, Zhu LQ (2019) MiR-21-5p/dual-specificity phosphatase 8 signalling mediates the anti-inflammatory effect of haem oxygenase-1 in aged intracerebral haemorrhage rats. Aging Cell 18:e13022.

Paxinos G, Watson C (1986) The rat brain in stereotaxic coordinates. Sydney: Academic Press.

Percie du Sert N, Ahluwalia A, Alam S, Avey MT, Baker M, Browne WJ, Clark A, Cuthill IC, Dirnagl U, Emerson M, Garner P, Holgate ST, Howells DW, Hurst V, Karp NA, Lazic SE, Lidster K, MacCallum CJ, Macleod M, Pearl EJ, et al. (2020) Reporting animal research: Explanation and elaboration for the ARRIVE guidelines 2.0. PLoS Biol 18:e3000411.

Ren H, Han R, Chen X, Liu X, Wan J, Wang L, Yang X, Wang J (2020a) Potential therapeutic targets for intracerebral hemorrhage-associated inflammation: an update. J Cereb Blood Flow Metab 40:1752-1768.

Ren JX, Sun X, Yan XL, Guo ZN, Yang Y (2020b) Ferroptosis in neurological diseases. Front Cell Neurosci 14:218.

Rocha E, Rouanet C, Reges D, Gagliardi V, Singhal AB, Silva GS (2020) Intracerebral hemorrhage: update and future directions. Arq Neuropsiquiatr 78:651-659.

Seibt TM, Proneth B, Conrad M (2019) Role of GPX4 in ferroptosis and its pharmacological implication. Free Radic Biol Med 133:144-152.

Sembill JA, Huttner HB, Kuramatsu JB (2018) Impact of recent studies for the treatment of intracerebral hemorrhage. Curr Neurol Neurosci Rep 18:71.

Shaw DJ, Seese R, Ponnambalam S, Ajjan R (2014) The role of lectin-like oxidised low-density lipoprotein receptor-1 in vascular pathology. Diab Vasc Dis Res 11:410-418.

Son Y, Kim S, Chung HT, Pae HO (2013) Reactive oxygen species in the activation of MAP kinases. Methods Enzymol 528:27-48.

Stankova TR, Delcheva GT, Maneva AI, Vladeva SV (2019) Serum levels of carbamylated LDL, nitrotyrosine and soluble lectin-like oxidized low-density lipoprotein receptor-1 in poorly controlled type 2 diabetes mellitus. Folia Med (Plovdiv) 61:419-425.

Stockwell BR, Jiang X, Gu W (2020) Emerging mechanisms and disease relevance of ferroptosis. Trends Cell Biol 30:478-490.

Takemura Y, Okamoto M, Hasegawa M, Hatanaka K, Kubota S (2019) Protamine may have anti-atherogenic potential by inhibiting the binding of oxidized-low density lipoprotein to LOX-1. Biosci Biotechnol Biochem 83:1094-1101.

Wan J, Ren H, Wang J (2019) Iron toxicity, lipid peroxidation and ferroptosis after intracerebral haemorrhage. Stroke Vasc Neurol 4:93-95.

Wang H, Peng S, Cai J, Bao S (2021) Silencing of PTPN18 induced ferroptosis in endometrial cancer cells through p-P38-mediated GPX4/xCT down-regulation. Cancer Manag Res 13:1757-1765.

Wang Y, Chen Q, Shi C, Jiao F, Gong Z (2019) Mechanism of glycyrrhizin on ferroptosis during acute liver failure by inhibiting oxidative stress. Mol Med Rep 20:4081-4090.

Wang Z, Zhou F, Dou Y, Tian X, Liu C, Li H, Shen H, Chen G (2018) Melatonin alleviates intracerebral hemorrhage-induced secondary brain injury in rats via suppressing apoptosis, inflammation, oxidative stress, DNA damage, and mitochondria injury. Transl Stroke Res 9:74-91.

Wei TH, Hsieh CL (2020) Effect of acupuncture on the p38 signaling pathway in several nervous system diseases: a systematic review. Int J Mol Sci 21:4693.

Wilkinson DA, Pandey AS, Thompson BG, Keep RF, Hua Y, Xi G (2018) Injury mechanisms in acute intracerebral hemorrhage. Neuropharmacology 134:240-248.

Xi T, Jin F, Zhu Y, Wang J, Tang L, Wang Y, Liebeskind DS, Scalzo F, He Z (2018) miR-27a-3p protects against blood-brain barrier disruption and brain injury after intracerebral hemorrhage by targeting endothelial aquaporin-11. J Biol Chem 293:20041-20050.

Yang G, Qian C, Zhang C, Bao Y, Liu MY, Jiang F, Li W, Liu Y, Ke Y, Qian ZM (2021) Hepcidin attenuates the iron-mediated secondary neuronal injury after intracerebral hemorrhage in rats. Transl Res 229:53-68.

Ye Q, Zeng C, Luo C, Wu Y (2020) Ferrostatin-1 mitigates cognitive impairment of epileptic rats by inhibiting P38 MAPK activation. Epilepsy Behav 103:106670.

Yu DR, Wang T, Huang J, Fang XY, Fan HF, Yi GH, Liu Q, Zhang Y, Zeng XZ, Liu QB (2020) MicroRNA-9 overexpression suppresses vulnerable atherosclerotic plaque and enhances vascular remodeling through negative regulation of the p38MAPK pathway via OLR1 in acute coronary syndrome. J Cell Biochem 121:49-62.

Yuan Y, Men W, Shan X, Zhai H, Qiao X, Geng L, Li C (2020) Baicalein exerts neuroprotective effect against ischaemic/reperfusion injury via alteration of NF-kB and LOX and AMPK/Nrf2 pathway. Inflammopharmacology 28:1327-1341.

Zhang H, Lu X, Hao Y, Tang L, He Z (2020a) MicroRNA-26a-5p alleviates neuronal apoptosis and brain injury in intracerebral hemorrhage by targeting RAN binding protein 9. Acta Histochem 122:151571.

Zhang J, Malik A, Choi HB, Ko RW, Dissing-Olesen L, MacVicar BA (2014) Microglial CR3 activation triggers long-term synaptic depression in the hippocampus via NADPH oxidase. Neuron 82:195-207.

Zhang Y, Fan BY, Pang YL, Shen WY, Wang X, Zhao CX, Li WX, Liu C, Kong XH, Ning GZ, Feng SQ, Yao X (2020b) Neuroprotective effect of deferoxamine on erastininduced ferroptosis in primary cortical neurons. Neural Regen Res 15:1539-1545.

Zhang Y, Hu M, Jia W, Liu G, Zhang J, Wang B, Li J, Cui P, Li X, Lager S, Sferruzzi-Perri AN, Han Y, Liu S, Wu X, Brännström M, Shao LR, Billig H (2020c) Hyperandrogenism and insulin resistance modulate gravid uterine and placental ferroptosis in PCOS-like rats. J Endocrinol 246:247-263.

Zhang Z, Wu Y, Yuan S, Zhang P, Zhang J, Li H, Li X, Shen H, Wang Z, Chen G (2018) Glutathione peroxidase 4 participates in secondary brain injury through mediating ferroptosis in a rat model of intracerebral hemorrhage. Brain Res 1701:112-125.

Zhou SY, Cui GZ, Yan XL, Wang X, Qu Y, Guo ZN, Jin H (2020) Mechanism of ferroptosis and its relationships with other types of programmed cell death: insights for potential interventions after intracerebral hemorrhage. Front Neurosci 14:589042.

Zhou Y, Wang Y, Wang J, Anne Stetler R, Yang QW (2014) Inflammation in intracerebral hemorrhage: from mechanisms to clinical translation. Prog Neurobiol 115:25-44.

P-Reviewer: Donato R; C-Editor: Zhao M; S-Editors: Yu J, Li CH; L-Editors: Yu J, Song LP; T-Editor: Jia Y

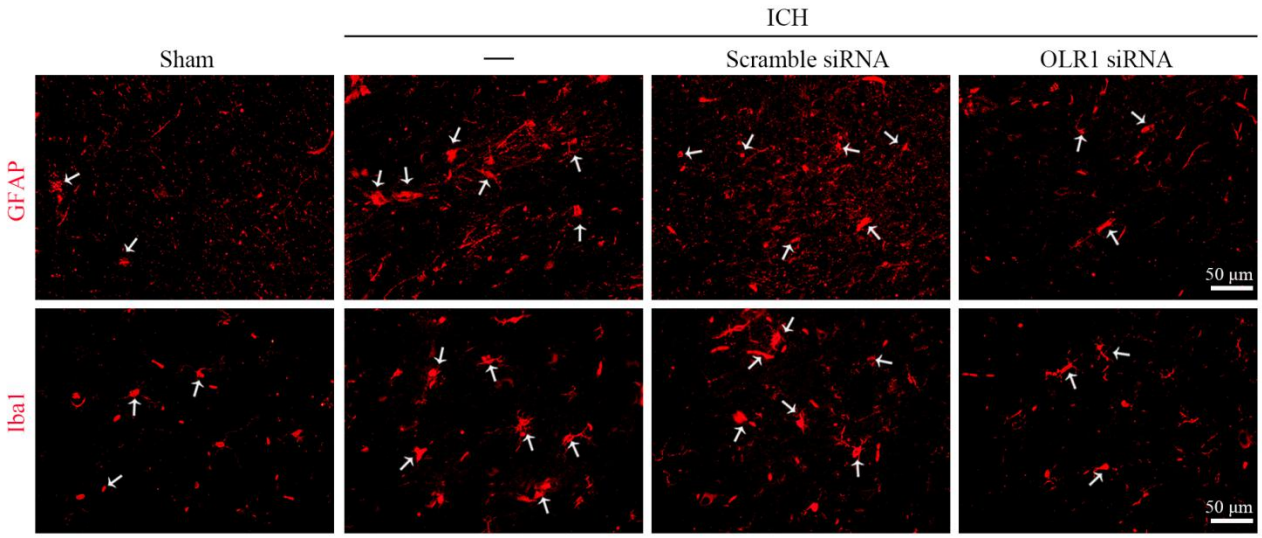

Additional Figure 1 Representative immunofluorescence staining to identify GFAP- or Iba1-positive cells.
The GFAP-positive and Iba1-positive cells were labeled red by Cy3, respectively. White arrows indicate the GFAP-positive or Iba1-positive cells. The loss of OLR1 reverted the elevated levels of GFAP and Iba1 in brain tissues induced by ICH. The experiments were repeated by six times. Scale bar: 50 μm. GFAP: Glial fibrillary acidic protein; Iba1: ionized calcium-binding adaptor molecule 1; ICH: intracerebral hemorrhage; OLR1: oxidized low-density lipoprotein receptor 1; siRNA: small interfering RNA.

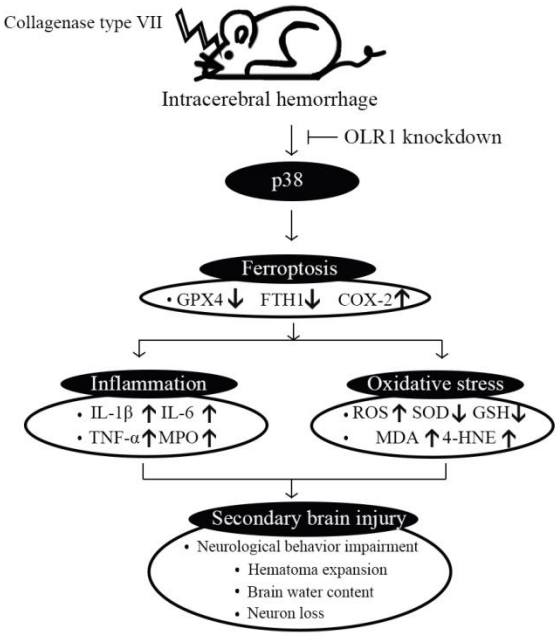

Additional Figure 2 The mechanism graph of OLR1/p38 axis and ferroptosis involves in the protective effects of ICH.

The OLR1 silence protected post-ICH brain tissues from the secondary brain injury by the inhibition of ferroptosis, which might be mediated by the downregulation of p38 signaling pathway. COX-2: Cyclooxygenase-2; FTH1: ferritin heavy polypeptide 1; GPX4: glutathione peroxidase 4; GSH: glutathione; IL: interleukin; MDA: malondialdehyde; MPO: myeloperoxidase; OLR1: oxidized low-density lipoprotein receptor 1; ROS: reactive oxygen species; SOD: superoxide dismutase; TNF-α: tumor necrosis factor-α; 4-HNE: 4-hydroxynonenal.